



Rain erosivity map for Germany derived from contiguous radar rain data

Franziska K. Fischer^{1,2,3}, Tanja Winterrath⁴, Karl Auerswald¹

¹Lehrstuhl für Grünlandlehre, Technische Universität München, Freising, 85354, Germany

5 ²Bayerische Landesanstalt für Landwirtschaft, Freising, 85354, Germany

³Außenstelle Weihenstephan, Deutscher Wetterdienst, Freising, 85354, Germany

⁴Deutscher Wetterdienst, Department of Hydrometeorology, Offenbach/ Main, 63067, Germany

10 *Correspondence to:* Karl Auerswald (auerswald@wzw.tum.de)

Abstract. Erosive rainfall varies pronouncedly in time and space. Severe events are often restricted to a few square kilometers. Rain radar data with high spatio-temporal resolution enable this pattern of erosivity to be portrayed for the first time. We used radar data collected with a spatial resolution of 1 km² for 452 503 km² to derive a new erosivity map for Germany and to analyze the seasonal distribution of erosivity. Extraordinarily large filtering was necessary to extract the expected long-term regional pattern from the scattered pattern of events. Filtering included averaging 2001 to 2017 and smoothing in time and space. The pattern of the resulting map generally agreed well with the previous map based on regressions of rain gauge data (mainly from the 1960s to 1980s). The pattern was predominantly shaped by orography. However, the new map has more detail; it deviates in some regions where the regressions previously used were weak; most importantly, it shows that erosivity is about 66% higher than in the map previously used. This increase in erosivity was confirmed by long-term data from rain gauge stations used for the previous map. The change was thus not caused by using a different methodology but by weather changes that may already be a dramatic result of climate change since the 1970s. Furthermore, the seasonal distribution of erosivity showed that more erosivity falls during the winter period when soil cover by plants is usually poor. For many crops higher erosion therefore also results from the change in seasonality. Predicted soil erosion in winter wheat is now about four times higher than in the 1970s due to the seasonal changes, combined with the increased erosivity. These topical erosivity data with high resolution will thus have definite consequences for agricultural advisory services, landscape planning and even political decisions.

1 Introduction

Soil erosion by heavy rain is regarded as the largest threat to the soil resource. Rain erosivity, which is a rain's ability to detach soil particles and provide transport by runoff, is one of the factors influencing soil erosion. The most commonly used measure of rain erosivity is the R factor from the Universal Soil Loss Equation USLE (Wischmeier, 1959; Wischmeier and Smith, 1958, 1978), although other concepts also exist (Morgan et al., 1999; Schmidt, 1991; Williams and Berndt, 1977).



The R factor is given as the product of a rain's kinetic energy and its maximum 30-min intensity. Both components are usually derived from hyetographs recorded by rain gauges. Such rain gauge data are spatially scarce. For instance, in Germany only one rain gauge per 2571 km² was available for the R map presently in use (Sauerborn, 1994). Hence, information has to be interpolated to derive an R map that enables R to be estimated for any location. Different interpolation techniques have been applied. Correlations (transfer functions) to other meteorological data available at higher spatial density were used the most (for an overview see Nearing et al., 2017). The German R-factor map is based on correlations between R and normal-period summer rainfall or normal-period annual rainfall, differing between federal states (Rogler and Schwertmann, 1981; Sauerborn, 1994, and citations therein).

Recent research has shown that the erosivity of single events exhibits enormous gradients in space (Fiener and Auerswald, 2009; Fischer et al., 2016; Fischer et al., 2018; Krajewski et al, 2003; Pedersen et al., 2010; Peleg et al., 2016), which is due to the small spatial extent of convective rain cells typical for erosive rains. The resulting heterogeneity has two consequences. First, interpolation between two neighboring rain stations will not be possible for individual rains because a rain cell in between may be completely missed. Second, even long records of rain gauge data may miss the largest events that occurred in close proximity to a rain gauge and thus underestimate rain erosivity. This is illustrated nicely by the data of Fischer et al. (2018). They showed that the largest event erosivity, which was recorded by contiguous measurements over only two months, was more than twice as large as the largest erosivity that occurred during 16 years when the same area was covered by 115 rain gauges. Furthermore, this single event contributed about 20 times as much erosivity as the expected long-term average. Even in a 100-yr record this single event would thus still change the long-term average erosivity. The large variability then directly translates to soil loss. This may be illustrated by soil loss measurements in vineyards in Germany. Emde (1992) found a mean soil loss of 151 t ha⁻¹ yr⁻¹ averaged over 10 plot years while Richter (1991) only measured 0.2 t ha⁻¹ yr⁻¹, averaged over 144 plot years. The difference is due to the largest event during the study by Emde (1992), which obviously had too much influence on the mean compared to the size of his data set. Such an event was missing entirely in Richter's (1991) much larger data set. The inclusion of rare events when measured by chance by a rain gauge leads to statistical problems due to their extraordinary magnitude. Unstable and unreliable transfer functions result that differ pronouncedly depending on whether a large event is included or not. To avoid this, Rogler and Schwertmann (1981) excluded all events for which the estimated return period was more than 30 yr (assuming that event erosivities followed a Gumble distribution), prior to the development of their transfer function. This approach must underestimate erosivity and, in turn, soil erosion because the largest events are then replaced by zero.

The demand for contiguous rain data to create R-factor maps has only recently been able to be met by radar rain data of high spatial and temporal resolution. Put simply, the measurements are based on the principle that radar beams are reflected by hydrometeors. The intensity of the reflection depends on rain intensity and the travel time of the reflected radar beam depends on the distance between the emitting and receiving radar tower and the hydrometeor. Radars usually measure with a resolution of approx. 1° azimuth and 125 to 250 m in the direction of beam propagation. The data are then typically



transformed to grids of square pixels of 1 km² (Bartels et al., 2004; Fairman et al., 2015), 4 km² (Koistinen & Michelson, 2002; Michelson et al., 2010) or 16 km² (Hardegree et al., 2008) after many refinement steps.

In this study, we used the new RW product from the radar climatology RADKLIM from the German Meteorological Service (Deutscher Wetterdienst, DWD). RW data provide gauge-adjusted and further refined precipitation for a pixel size of 1 x 1
5 km² (Winterrath et al., 2017, 2018). RW data of 17 yr (2001 – 2017) are available as a contiguous source of rain information. Using these data to establish a new R-factor map for Germany should be a major step forward compared to the existing map, which was derived from an inconsistent set of data compiled by different researchers (e.g., some had winter precipitation data available and used it while others did not; see Sauerborn, 1994) and with equations developed independently for 16 federal states. Our data set is much larger (by a factor of 2571 regarding locations) and, because of the contiguous data
10 source, it does not require interpolation with transfer functions. We expect that there will be considerable changes in the pattern of erosivity due to the removal of transfer-function weaknesses. We also expect that the R-factor map will exhibit higher values than the existing map, for two reasons. Very large and rare events will no longer be missed, as occurred previously due to the large distances between meteorological stations, and there is no longer any need to remove these events to arrive at robust transfer functions. The second reason for higher R factors is due to global climate change, as Rogler and
15 Schwertmann (1981) and Sauerborn (1994) mostly used data from the 1960s, 1970s and 1980s. Global climate change is expected to increase rain erosivity (Burt et al., 2016).

2 Material and methods

2.1 Radar-based precipitation data

DWD runs a Germany-wide network of, at present, 17 C-Band Doppler radar systems (Fig. 1). This network underwent
20 several upgrades during the analysis period. At the start of the time period considered, five single-polarization systems (DWSR-88C, AeroBase Group Inc., Manassas, USA) were operated without a Doppler filter, the latter being added between 2001 and 2004. Between 2009 and 2017, DWD replaced the network of C-band single-polarization systems of the types METEOR 360 AC (Gematronik, Neuss, Germany) and DWSR-2501 (Enterprise Electronics Corporation, Enterprise, USA) with modern dual-polarization C-band systems of the type DWSR-5001C/SDP-CE (Enterprise Electronics Corporation), all
25 equipped with Doppler filters. During this period, a portable interim radar system of the type DWSR-5001C was installed at some sites.

The radar systems permanently scan the atmosphere to detect precipitation signals. Every five minutes, the radars perform a precipitation scan, each with terrain-following elevation angle to measure precipitation near the ground. The resulting local reflectivity information over a range of 128 km is combined to form a Germany-wide mosaic of about 1100 km in the north-
30 south and 900 km in the west-east direction. The reflectivity information is converted to precipitation rates applying a reflectivity–rain rate (ZR) relationship. An operational quality control system screens the radar data. To further improve the quantitative precipitation estimates, the radar-derived precipitation rates are summed to hourly totals and immediately



adjusted to gauge data resulting in RADOLAN (i.e. online-adjusted, radar-derived precipitation), which provides precipitation data in real time, mainly for applications in flood forecasting and flood protection (Bartels et al., 2004; Winterrath et al., 2012).

Based on RADOLAN, the climate version RADKLIM is derived. Compared to the real-time approach, the data are additionally offline-adjusted to daily gauge data, combining a total of more than 4400 rain gauges measuring hourly and daily (1 rain gauge per 80 km²). The data are then reprocessed by new climatological correction methods, e.g. for spokes, clutter or short data gaps. Spokes result from permanent obstacles blocking the radar beam, while clutter is introduced by non-meteorological targets like windmills or birds. The final product (RW data) has a temporal resolution of 1 h and a spatial resolution of 1 km x 1 km in polarstereographic projection. For more detailed information on RADKLIM the reader is referred to Winterrath et al. (2017). The RW data, restricted to the German territory, are freely available (Winterrath et al., 2018). For the first time, the RADKLIM data set provides contiguous precipitation data with high temporal and spatial resolution. It includes local heavy precipitation events that are partly missed by point measurements alone. Thus, it particularly improves the analysis of extreme precipitation events.

Two additional data sets were used to verify the validity of the approach and to examine effects of methodological details (see below). These data sets are erosivities derived from radar data at 5-min resolution taken from Fischer et al. (2016) and erosivities derived from 115 rain-gauge station data in Germany during 2001 to 2016, which were taken from Fischer et al. (2018).

2.2 Erosivity calculation procedures

According to Wischmeier (Wischmeier, 1959; Wischmeier and Smith, 1958, 1978), the erosivity of a single rain event (R_e) is the product of the maximum 30-min rain intensity ($I_{\max30}$) and the total kinetic energy (E_{kin}). For hyetographs recorded by rain gauges, an erosive rain event is defined as a total precipitation amount (P) of at least 12.7 mm or an $I_{\max30}$ of more than 12.7 mm h⁻¹ that is separated from the next rain by at least six hours.

$$R_e = I_{\max30} * E_{\text{kin}} \quad (1)$$

Kinetic energy $E_{\text{kin},i}$ per mm rain depth (in kJ m⁻² mm⁻¹) is given for intervals i of constant rain intensity I :

$$E_{\text{kin},i} = (11.89 + 8.73 * \log_{10} I) * 10^{-3} \quad \text{for } 0.05 \text{ mm h}^{-1} \leq I < 76.2 \text{ mm h}^{-1} \quad (2.1)$$

$$E_{\text{kin},i} = 0 \quad \text{for } I < 0.05 \text{ mm h}^{-1} \quad (2.2)$$

$$E_{\text{kin},i} = 28.33 * 10^{-3} \quad \text{for } I \geq 76.2 \text{ mm h}^{-1} \quad (2.3)$$

For all intervals i , $E_{\text{kin},i}$ is multiplied with the rain amount of this interval and then summed to yield E_{kin} for the entire event. The annual erosivity of a specific year is the R_e sum of all n erosive events within this year. The average annual erosivity (R) is then the average of all annual erosivities during the study period (17 yr in this case). While in the USA and other countries the unit MJ mm ha⁻¹ h⁻¹ is often used for R_e , we use N h⁻¹ because it is the unit most often used in Europe and because of its



simplicity. Both units can be easily converted by multiplying the values in N h^{-1} with a factor of 10 to yield $\text{MJ mm ha}^{-1} \text{ h}^{-1}$. The unit for R is then $\text{N h}^{-1} \text{ yr}^{-1}$.

Rain erosivity strongly depends on intensity peaks. Fischer et al. (2018) have shown that these peaks increasingly disappear the lower the spatial and temporal resolution becomes. This can be accounted for by scaling factors but these scaling factors can only adjust to an average behavior, while the influence of the true event R_e may either be too large or too small. A high spatio-temporal resolution should be used to determine R_e for individual events. To determine the long-term average pattern, i.e. an R-factor map for planning and prediction purposes, using data with lower resolution and applying appropriate scaling factors is advantageous because this will reduce the noise introduced by large events of small spatial extent that would not be leveled out by averaging alone. We will use data in 1-h time increments, which additionally have the advantages that they are adjusted to rain gauge measurements and the amount of data is reduced by a factor of 12 compared to 5-min increments. This is especially important when all calculations, including identification of rain breaks > 6 h and periods of $I_{\text{max}30}$, have to be carried out for many years and many locations. In our case, roughly 7×10^{10} 1-h increments had to be processed.

Gaps in the time series have been considered when calculating mean R factors by scaling the total sum of erosivity over the whole time series to 365.25 days. If the effective number of missing values exceeded two months per year, the respective year was excluded from the calculation for that pixel.

According to Fischer et al. (2018), the following modifications in the calculation of R_e had to be made to account for the temporal resolution of 1 h, the spatial resolution of 1 km^2 and radar measurement: (i) $I_{\text{max}30}$ was replaced by the maximum 1-h rain depth and the threshold was lowered to 5.8 mm h^{-1} , while the total precipitation threshold remained at 12.7 mm . (ii) Rain breaks separated events when five subsequent 1-h intervals without rain occurred. This assumed that rain events stop and start on average in the middle of the first and the last non-zero rain interval, yielding a total rain break of 6 h. (iii) The temporal scaling factor was 1.9 and the spatial scaling factor was 1.13, to which 0.35 has to be added to account for the radar measurement instead of the rain gauge measurement. The total scaling factor $[(1.13 + 0.35) \times 1.9]$ was then 2.81.

2.2 Generating a Germany-wide R-factor map

The reduction of noise by using 1-h increments was still not sufficient to level out the most extreme events. Two further filtering steps were therefore applied, in addition to using a 17-yr mean. The first averaging step was to winsorize the annual erosivities of the 17 yr (Dixon and Yuen, 1974) for each individual pixel by replacing the lowest value with the second-lowest value and the highest value with the second-highest value. Winsorizing is an appropriate measure for calculating a robust estimator of the mean in symmetrically distributed data but it is biased for long-tailed variables like rain erosivity. Thus, the country-wide mean of all winsorized data ($96 \text{ N h}^{-1} \text{ yr}^{-1}$) was lower than the mean of the original data ($98 \text{ N h}^{-1} \text{ yr}^{-1}$). In order to remove this bias, we binned all data in 26 bins of $20 \text{ N h}^{-1} \text{ yr}^{-1}$ width and calculated the mean R before and after winsorizing. For bins with $R < 180 \text{ N h}^{-1} \text{ yr}^{-1}$, comprising 95% of all pixels, the bias increased linearly with R ($r^2 = 0.92$; $n = 8$) and amounted to 2.3% of R. Above $180 \text{ N h}^{-1} \text{ yr}^{-1}$ there was no further increase in the bias ($r^2 = 0.01$, $n = 18$),



which was, on average, $3.4 \text{ N h}^{-1} \text{ yr}^{-1}$. We removed the bias by adding 2.3% to all values $< 180 \text{ N h}^{-1} \text{ yr}^{-1}$ and $3.4 \text{ N h}^{-1} \text{ yr}^{-1}$ to all values above.

The third noise-reduction step applied geostatistical methods. A semivariogram (over a range of 50 km) was calculated and ordinary kriging was applied. Geostatistical analysis was done in R (version 3.5.0; R Core Team, 2018) using gstat (Gräler et al., 2016). To remove noise, a block size of $10 \times 10 \text{ km}^2$ was chosen, while the spatial resolution remained at 1 km. This step was also necessary to fill pixels with data gaps of more than one year (0.6% of the entire area). The missing information was obtained from neighbor pixels. The radar data extended beyond German borders. In total, 452 503 pixels were used to ensure low krige errors near borders or on islands, while the final map was restricted to the German land surface (357 779 pixels). Using 1-h data instead of 5-min data reduced the effect of single extreme events at certain locations. Winsorizing reduced the effect of extreme years at a location, in addition to the effect of averaging 17 yr. Finally, kriging used the information from neighbor pixels to reduce the effect of the extremes. This should not have affected the regional pattern. To evaluate whether this was the case and to quantify the effect of all smoothing steps, we used the data from Fischer et al. (2016), who calculated rain erosivity from 5-min-resolution radar data for two years (2011 and 2012) and an area of $14\,358 \text{ km}^2$ (yielding a total of 28 770 pixel years), called “test region” in the following. Using these data we calculated semivariograms after each smoothing step from annual to biennial erosivities based on 5-min and 1-h resolution, for 17-yr average erosivities, for winsorized averages and finally for kriged values. Smoothing should reduce the influence of individual violent thunderstorm cells and reveal the regional pattern. In geostatistical analysis this decreases the sill of the semivariogram while the range increases as it changes from being dominated by thunderstorm cells to being dominated by the regional pattern.

2.3 Return periods

Rain erosivity usually follows long-tailed distributions, which leads to the question of how frequent years of extraordinarily large erosivity are, which requires the development of cumulative distribution curves (for basic concepts see Stedinger et al., 1993). Seventeen years are not sufficient to reliably estimate a cumulative distribution curve for every pixel. We combined all data (452 503 pixels and 17 yr) after expressing the event erosivities of all individual years relative to the winsorized and bias-corrected mean of each pixel (in percent). This enabled the cumulative distribution curves to be calculated from a large data set ($n = 7.7$ million) and the expected maximum relative annual erosivity for a given return period to be estimated from the complementary cumulative distribution curve (exceedance). This was also done for the relative annual erosivities of the test region, calculated from 1-h rain data, to examine whether the general cumulative distribution curve also applies to smaller regions.

The erosivities, when calculated from 1-h rain data, are already smoothed and do not adequately reflect the extremes that result from data that are more highly resolved, such as the 5-min rain data. The cumulative distribution curve for the test region was also calculated using the 5-min rain data. Given that the cumulative distribution curves of the entire study area and the test region agree for the relative erosivities calculated from 1-h data, this can also be expected to be the case for the



relative erosivities calculated from 5-min rain data. The cumulative distribution curve for the test region calculated from 5-min data will then be a fair estimate of the return periods anywhere in the research area.

2.4 Annual cycle of rain erosivity

The seasonal variation, calculated as the relative contribution of each day to total erosivity, is called erosion index distribution or EI distribution (Wischmeier and Smith, 1978). It is required in erosion modeling to determine the influence of seasonally varying soil cover due to crop development. The convolution of the seasonal effect of soil cover with the seasonal EI distribution results in the so-called crop and cover factor (C factor). The EI distribution was calculated for each pixel and averaged over all 452 503 pixels. Seventeen years of data still did not suffice to show similar amounts of erosivity on subsequent days, despite the large number of pixels. There was still considerable scatter that required smoothing to illustrate the seasonal distribution. Smoothing between individual days during the year involved three steps (for details of the methods see Tukey, 1977): first a 13-d centered median was calculated for each day. A centered median preserves the common trend signal and the level shifts in the smooth (Gallagher and Wise, 1981), which is also true for the two subsequent steps. A 3-d skip mean (leaving out the second day) was calculated from the results, followed by a 25-d centered hanning mean (weighted mean with linearly decreasing weights). The year was recycled to allow the smoothing methods to be applied at the boundaries.

The EI distribution deviated from the EI distribution used previously. This was especially pronounced during the winter months. However, radar measurements tend to have larger errors during wintertime with snowfall. The reduced reflectivity of snow particles may lead to an underestimation of the precipitation rate, while the increased reflectivity of melting particles in the bright band may cause an overestimation. Moreover, the lower boundary layer promotes a potential overshooting of the radar beam with regard to the precipitating cloud. Therefore, we also calculated the EI distribution using data from 115 rain gauges distributed throughout Germany and covering 2001 to 2016. These data were taken from Fischer et al. (2018). This data set will also be used in the discussion for comparison of recent radar-derived erosivities with recent raingauge-derived erosivities and with historic raingauge-derived erosivities taken from literature.

3 Results

3.1 Erosivity map

The regional pattern (Fig. 2) was mainly determined by orography. Highest values (above $185 \text{ N h}^{-1} \text{ yr}^{-1}$) were found in the very south where the northern chain of the Alps reaches altitudes of almost 3000 m above sea level (a.s.l.). Smaller mountain ranges are also characterized by high mean annual erosivities. For instance, the Bavarian Forest, in the southeast on the Czech border with elevations of up to 1450 m a.s.l., exhibited annual erosivities of above $155 \text{ N h}^{-1} \text{ yr}^{-1}$. The Ore Mountains in the east also on the Czech border, with elevations of up to 1244 m a.s.l., had erosivities mostly between 125 and $155 \text{ N h}^{-1} \text{ yr}^{-1}$. Also mountain ranges like the Black Forest (a mountain range in southwestern Germany oriented north-south) or the



Harz Mountains (an area of high erosivities located almost in the middle of northern Germany) clearly shape the erosivity map. Upwind-downwind effects were detectable. For example, the areas west-north-west (upwind) of the Harz Mountains had erosivities of between 70 and 80 $\text{N h}^{-1} \text{yr}^{-1}$, while the areas east-south-east (downwind) received less than 65 $\text{N h}^{-1} \text{yr}^{-1}$.

3.2 The effects of smoothing

5 Winsorizing reduced the standard deviation (SD) of a pixel over time from, on average, 49 $\text{N h}^{-1} \text{yr}^{-1}$ to 39 $\text{N h}^{-1} \text{yr}^{-1}$, while bias correction left the mean for all pixels unchanged at 98 $\text{N h}^{-1} \text{yr}^{-1}$. Using kriging, the mean remained the same at 98 $\text{N h}^{-1} \text{yr}^{-1}$, because kriging is an unbiased linear interpolator that smoothed locally (over distances of about 10 to 15 km). Only the very extreme values disappeared. Values lower than 45 $\text{N h}^{-1} \text{yr}^{-1}$, which had contributed 0.06% to the winsorized data, disappeared. In addition, values larger than 450 $\text{N h}^{-1} \text{yr}^{-1}$, which had contributed 0.03% to the winsorized data, also
10 disappeared.

Rain erosivity from 5-min resolution data for the test region showed large small-scale variability, even for annual sums of erosivity (Fig. 3, upper panel). The range was only 20 km, indicating that the annual pattern was dominated by individual cells of violent rain. The semivariance for a lag of 20 km was 2749 $\text{N}^2 \text{h}^2 \text{yr}^{-2}$ (Table 1). Using the normal distribution, in 31.8% of all cases the difference between two pixels separated by 20 km must then be larger than 52 $\text{N h}^{-1} \text{yr}^{-1}$ (square root
15 of 2749 $\text{N}^2 \text{h}^2 \text{yr}^{-2}$), which is more than half the average annual erosivity in Germany. After averaging both years (2011 and 2012), the semivariance for a lag of 20 km was reduced to 1569 $\text{N}^2 \text{h}^2 \text{yr}^{-2}$ and the range stayed the same at approximately 20 km. Both findings indicated that even after averaging two years, the individual cells of violent rain were still fully detectable and had not merged to form a larger pattern.

The effect when using data with a resolution of 1 h was almost as strong as when two years were averaged. Semivariance at
20 a lag of 20 km was only 1667 $\text{N}^2 \text{h}^2 \text{yr}^{-2}$ for annual values and 953 $\text{N}^2 \text{h}^2 \text{yr}^{-2}$ for biannual averages. Even more importantly, due to smoothing of the extreme events, the regional trend became better visible. This trend is evident from the gradual increase in semivariance over the entire range of lags shown in Fig. 3. This regional trend was already detectable in the annual erosivities calculated from 5-min data (Table 1), but did not appear to be significant due to the large semivariance caused by cells of violent rain. Importantly, smoothing using 1-h data did not change overall erosivity. The biannual average
25 for the test region was 115 $\text{N h}^{-1} \text{yr}^{-1}$ when calculated from 5-min data and 114 $\text{N h}^{-1} \text{yr}^{-1}$ when calculated from 1-h data.

Averaging 17 yr further reduced variability (Fig 3, upper panel). Semivariance strongly decreased to 197 $\text{N}^2 \text{h}^2 \text{yr}^{-2}$ and the influence of individual cells of violent rain became small relative to the regional trend, leading to an almost linear increase in semivariance over distance. The influence of extraordinary years in individual pixels was further reduced by winsorizing, which slightly reduced semivariance at 20 km distance to 190 $\text{N}^2 \text{h}^2 \text{yr}^{-2}$.

30 Finally, kriging reduced semivariance at 20 km distance to 121 $\text{N}^2 \text{h}^2 \text{yr}^{-2}$, leaving mainly the regional trend. Thus, the step from 5-min to 1-h resolution reduced semivariance at 20 km by a factor of 1.6; averaging 17 yr reduced semivariance by a factor of 8.5; winsorizing contributed a factor of 1.04 and kriging a factor of 1.6. In total, semivariance was reduced by a factor of 23, indicating a pronounced patchiness of erosive rains on the annual scale that could not be leveled out by



averaging 17 years alone. These factors became larger at shorter distances (e.g. the combined factor was 32 for a lag of 10 km) because the importance of thunderstorm cells, relative to the regional trend, increased. Correspondingly, the combined effect decreased with increasing distance (e.g., the factor was only 13 for a lag of 40 km) because the regional trend, which was not removed by the smoothing procedures, became increasingly important. The regional trend, extracted from the change in semivariance between lags of 20 km and 40 km, remained practically unchanged at $0.2 \text{ N h}^{-1} \text{ yr}^{-1} \text{ km}^{-1}$, independent of the degree of smoothing (Table 1). In contrast, the effect of violent rain cells decreased greatly from $2.4 \text{ N h}^{-1} \text{ yr}^{-1} \text{ km}^{-1}$ to $0.3 \text{ N h}^{-1} \text{ yr}^{-1} \text{ km}^{-1}$.

After winsorizing and kriging, the semivariances for the test region followed a linear regression through the origin almost perfectly ($r^2 = 0.9889$, $n = 50$). This indicated that the variation in erosivity over a distance of 50 km followed linear trends without any noise (nugget) or small-range structures that could be attributed to individual cells of violent rain. The semivariances, when calculated for the whole of Germany, were considerably higher (twice as high at a lag of 50 km; Fig. 3, lower panel) and close to a linear trend only for short distances (e.g. a linear regression through the origin for the first 15 km yielded $r^2 = 0.9905$). For larger distances, the semivariogram followed an exponential model (nugget $4 \text{ N}^2 \text{ h}^{-2} \text{ yr}^{-2}$, partial sill $970 \text{ N}^2 \text{ h}^{-2} \text{ yr}^{-2}$, effective range 123 km). The inclusion of mountain areas with high erosivities and steep erosivity gradients that were missing in the test region led to both the higher semivariance and the exponential model.

3.3 Return periods

The cumulative distribution of the relative annual erosivities followed a straight line in a probability plot fairly well when the logarithm was used (Fig. 4), indicating a log-normal distribution (log mean 1.96; log SD 0.19). A very similar cumulative distribution was found for annual values derived from the 1-h data of the test region (log mean 1.97; log SD 0.18), while the distribution was considerably wider for the less-smoothed 5-min data (log mean 1.94; log SD 0.22). The annual expected erosivity was 88%, 216% and 273% of the respective mean for return periods of 2 yr, 30 yr, and 100 yr when the 5-min data were used (Fig. 4). It is important to note that these values apply for averages of 1 km^2 pixels and include the smoothing that results from the radar measurement, the radar reprocessing, and from using 5-min rain increments. Even extremer years are expected to occur in reality.

3.4 Erosion index distribution

There was a pronounced peak in the relative seasonal variation during summer months (Fig. 5). The relative daily erosion index increased rapidly from mid-April to mid-May to a mean of $0.61 \% \text{ d}^{-1}$ in June, July and August, and declined rapidly again from mid-August to September. The contribution of winter months was small (mean of December, January, February, and March: $0.08 \% \text{ d}^{-1}$). Even more striking was the fact that this pattern required considerable smoothing to yield a continuous seasonal time course. The difference between subsequent days in the unsmoothed data was enormous (e.g., $1.5 \% \text{ d}^{-1}$, $0.4 \% \text{ d}^{-1}$ and $0.4 \% \text{ d}^{-1}$ on July 29, 30 and 31). This was despite the large number of measurements (17 yr and 455 309 pixels) that were averaged for each day. It highlights how extreme some violent rains must be. Despite the rather small



extent of individual erosivity cells, many of them occurred at the same day making a high relative contribution to total erosivity for this day. While particular days of the year are influenced by heavy precipitation, during other days no erosive rain fell anywhere within the research area. Seventeen years were not sufficient to level out the contrast between subsequent days. The results of the smoothing procedure show that even 221 yr (17 yr multiplied by a moving-average window of 13 d) would not be sufficient to level out these differences because two additional smoothing steps had to be applied to arrive at a smooth time course.

The EI distribution, when calculated from rain gauge data (1840 station years), was very similar to the distribution calculated from the much larger radar data set. This was especially true during winter months, when values derived from both measurement methods were considerably higher than expected.

10 4 Discussion

4.1 Increase in erosivity

The most striking difference between the German R map presently in use (Sauerborn, 1994) and the radar-derived map is a pronounced increase in erosivity. A German average of $58 \text{ N h}^{-1} \text{ yr}^{-1}$ was derived from the Sauerborn map (1994) (Auerswald et al., 2009), while the radar-based map suggests an average of $98 \text{ N h}^{-1} \text{ yr}^{-1}$. This will increase predicted soil losses by 69%. An almost identical increase resulted when the erosivity of meteorological stations, as reported by Sauerborn (1994), was compared with the erosivity derived from radar data at the same locations, which resulted in an increase of 63% (Fig. 6). Thus, the increase in erosivity is not an effect of the regression approach that was previously used or due to better capturing of extreme events by the contiguous radar data.

Fischer et al. (2018) calculated erosivity for 33 of the Sauerborn stations from recent (2001 to 2016) rain gauge data. A comparison of these data with the Sauerborn data (1994) also showed a similar increase of 52% (Fig. 5). The increase in erosivity between the Sauerborn map (1994) and the new radar-derived map is thus also not an artifact of using radar data but the result of a true change in erosivity over time. This is further corroborated by Fiener et al. (2013), who analyzed long-term records from ten meteorological stations in western Germany. They found an increase in erosivity of 63% between 1973 and 2007. Both independent findings leave little doubt that the pronouncedly higher values in the new erosivity map are a result of a change in weather properties and not a result of the difference in the applied methodologies, although we did expect the mean to increase due to the contiguous data set, which is better at recording rare extremes.

4.2 Change in the regional pattern

The regional patterns of the Sauerborn erosivity map (1994) that is currently used, and that of the radar-based map, generally agree well, but with two exceptions. First, the radar-based map shows distinctly higher values south-east of the German Bight where the air masses coming from the North Sea are channeled by the Elbe river estuary and its Pleistocene meltwater valley and then hit the higher areas of the North German moraines. A high frequency of large rains is not unlikely in this



situation. The reason that this was missed by Sauerborn (1994) using the data obtained by Hirche (1990) for Lower Saxony is mainly due to the low data density and the regression approach. Only 18 stations were available for the whole of Lower Saxony and only five of them were in the area of high erosivity. Using the 18 stations in the state of Lower Saxony only, and ignoring the difference between landscapes, resulted in a rather poor regression with long-term annual rainfall (r^2 was only 5 0.32), and therefore a large prediction error and considerable smoothing of the true erosivity pattern can be expected. For comparison: in Bavaria the regression with long-term rainfall yielded r^2 of 0.92 (Rogler and Schwertmann, 1981).

The second difference in the pattern is that the radar-derived map reveals more detail than the regression-based map by Sauerborn (1994). This is especially evident in southern Germany where southwest-northeast oriented structures seem to follow thunderstorm trains. In the north-east quarter of Germany, where the pattern is not shaped by mountain ranges, a 10 rather patchy pattern resulted. Although Sauerborn (1994) had already found a patchy pattern in this area it appears to be patchier now. It is, at present, difficult to decide whether this pattern is random due to large multi-cell clusters of rainstorms and will level out on the long term, or whether landscape properties, e.g. the existence of large forests, cause a stable pattern in an area where other factors affecting the pattern are missing. More detailed variation may also be expected in mountainous areas but radar measurements cannot adequately show this variation. In the future, using data obtained by commercial 15 microwave links as an additional source for retrieving precipitation (Chwala et al., 2012, 2016; Overeem et al., 2013) may improve high resolution estimates, particularly in these areas.

4.3 Change in the seasonal distribution of the erosion index

The third pronounced difference was found for the erosion index distribution needed for C-factor calculations. A change in the seasonality of erosivity was already suggested by Fiener et al. (2013) analyzing an 80-yr time series. However, Fiener et al. (2013) used data from April to October only, and their results therefore cannot be compared directly with our results that 20 show the most pronounced changes for the period from December to March.

At present, only the erosion index developed by Rogler and Schwertmann (1981) for Bavaria is used for C-factor calculations in Germany (e.g. Schwertmann et al., 1990; DIN, 2017), although unpublished erosion indices are also available for other federal states (e.g., Hirche, 1990). The index by Rogler and Schwertmann (1981) is characterized by very low 25 values during winter months, which in turn causes a sharp increase during summer months. In contrast, the radar-based index, although still having a pronounced summer maximum, predicts a higher percentage of erosivity during winter. Rogler and Schwertmann (1981) found that only 1.5% of the annual erosivity fell from January to March, while Fig. 5 indicates that these months contributed 6.9% to annual erosivity. This deviation may be caused by a regional variation in the erosion index because the unpublished indices for other federal states also suggested a higher contribution by winter months (e.g., January 30 to March contributed 7.5% in Lower Saxony according to Hirche, 1990). However, restricting our data set to Bavaria led to a very similar index during winter months (e.g., 6.2% for January to March) to the index for the whole of Germany and the discrepancy with Rogler and Schwertmann (1981) remained.



A second explanation is that the Rogler and Schwertmann data (1981) were too limited to capture enough erosive rains. This explanation is corroborated by the large scatter between individual days that still exists in our data set (Fig. 5), although our data set was more than 50 000 times larger than the data set used by Rogler and Schwertmann (1981).

A third explanation could again be climate change. In Germany extreme rainfall events have increased in winter by 463% during the last century with the trend greatest during the last few decades, while summer and autumn remained unchanged (Schönwiese et al., 2003).

The change in erosion index may be regarded as being rather unimportant at first glance because erosivity is still dominated by precipitation in summer. This small increase in erosivity during the winter months, however, could have important consequences for the C factor of crops that, due to their crop development stage, provide only a small amount of soil cover during the winter. As there is practically no growth during winter, these crops are susceptible to erosion over a long period and thus experience a considerable amount of erosivity, even though erosivity per day is low. Calculating the C factor for continuous winter wheat from the soil loss ratios and cropping-stage dates reported by Schwertmann et al. (1990) yields a C factor of 0.04 if the erosion index from Rogler and Schwertmann (1980) is used. The C factor increases to 0.10 when the erosion index in Fig. 5 is applied. Thus, the predicted soil loss for continuous wheat is more than twice as high as previously expected due to the change in the erosion index (and four times higher if the change in erosivity is also considered). While the C factor of the maize year in a typical maize-winter wheat rotation is currently regarded to be eight times higher than that of winter wheat, it is only four times higher when the new erosion index is applied. Furthermore, the C factor of the entire rotation increases by 15%.

4.4 Stochasticity

Soil erosion is characterized by a large temporal variability at a small spatial scale due to the stochastic character of erosive rains. About 20 yr are necessary, according to Wischmeier and Smith (1978), until this variability levels out and average soil loss approaches values predicted with the (R)USLE. Our data set covered 17 yr but significant additional smoothing was still necessary. This implies that 20 yr will still not be sufficient to level out extraordinary events. Most studies measuring soil erosion under natural rain use much shorter intervals that usually cover only a few years and rarely exceed ten years (see Auerswald et al., 2009, for a meta-analysis of German studies and Cerdan et al., 2010, for European studies). The interpretation of such short-term studies and the applicability of the results are limited due to the pronounced variability of natural rains.

We applied stepwise smoothing in order to minimize the disadvantages inherent in different smoothing procedures and to be able to smooth in time and space. We used rain data with hourly resolution instead of more highly resolved data and compensated for the disadvantages by using a scaling factor and by adjusting the threshold intensity according to Fischer et al. (2018). This procedure smoothed between individual rains. We added winsorizing and bias correction to smooth between years at a certain location. Finally, we added geostatistical smoothing to level out differences between neighboring locations caused by the small spatial extent of erosive rain cells. While the effects of winsorizing and geostatistical smoothing are



rather easy to assess, the effects are less clear when hourly resolved data are used, although the mean erosivity was identical for our test region when calculated with both resolutions. The pronounced influence of orography on the R-factor map could have, at least partly, been caused by this smoothing step. Orographic rainfall may increase hourly rainfall but it may not, to the same degree, increase high intensity peaks that exert a dominant influence on erosivity. Still, this is presently speculative because the high variability of erosive events means that this question cannot be answered using a 17-yr time series. In one or two decades the data series may be long enough to use data of 30-min or even 5-min resolution.

In addition, the erosion index required pronounced smoothing to improve representation of the seasonal variation. The shift of a certain crop stage by only one day can cause large discrepancies in the resulting C factor, depending on whether a day of large erosivity in the past is included or excluded at the bounds of the crop stage. Smoothing can prevent this. This is especially important for short crop stages, while the effect becomes small for longer periods. For instance, the monthly sums of the smoothed data correlated closely with the sums of the unsmoothed data (coefficient of determination: 0.995; Nash-Sutcliffe efficiency: 0.994).

5. Conclusions

Radar-derived rainfall enables highly resolved and contiguous maps of erosivity to be derived. This yielded a rain erosivity map with high spatial detail and avoided errors in landscapes with insufficient rain gauge density. The data showed that present (2001 to 2017) rain erosivity is considerably higher than previously expected. Furthermore, the seasonal distribution of rain erosivity also deviated from current expectations and indicated that winter months make a higher contribution to total erosivity than previously thought. Considerably more erosion can be expected for crops that are at a highly susceptible stage of development in winter. In consequence, the predicted soil loss will change pronouncedly by using radar-derived erosivity and the ranking of crops regarding their erosion potential will change. This will have definite consequences for agricultural extension and advisory services, landscape planning and even political decisions.

Author contribution

KA designed the analysis, which was mainly carried out by FF. TW provided most data and the knowledge about all steps involved in radar data creation. KA prepared the manuscript with contributions by FF and TW.

Acknowledgements

This study was part of the project “Ermittlung des Raum- und Jahreszeitmusters der Regenerosivität in Bayern aus radargestützten Niederschlagsdaten zur Verbesserung der Erosionsprognose mit der Allgemeinen Bodenabtragsgleichung” at the Bavarian State Research Center for Agriculture (PI Robert Brandhuber). It was funded by the Bayerisches Staatsministerium für Ernährung, Landwirtschaft und Forsten (A/15/17). The RADKLIM data were from the project



“Erstellung einer dekadischen radargestützten hochauflösenden Niederschlagsklimatologie für Deutschland zur Auswertung der rezenten Änderung des Extremverhaltens von Niederschlag (Kurztitel: Radarklimatologie)” financed by the Strategic Agencies’ Alliance “Adaptation to Climate Change” consisting of the Federal Office of Civil Protection and Disaster Assistance (BBK), the Federal Institute for Research on Building, Urban Affairs and Spatial Development (BBSR), the Bundesanstalt Technisches Hilfswerk (THW), the Umweltbundesamt (UBA), and the Deutscher Wetterdienst (DWD).
5 Melanie Treisch helped with ArcGIS operations, Karin Levin provided language editing, and Helmut Rogler has, for many years, requested that the German R-factor map be updated.

References

- Auerswald, K., Fiener, P., Dikau, R.: Rates of sheet and rill erosion in Germany – a meta-analysis. *Geomorph.*, 111, 182–193. <http://dx.doi.org/10.1016/j.geomorph.2009.04.018>, 2009.
- Bartels, H., Weigl, E., Reich, T., Lang, P., Wagner, A., Kohler, O., Gerlach, N.: Projekt RADOLAN: Routineverfahren zur Online-Aneicherung der Radarniederschlagsdaten mit Hilfe von automatischen Bodenniederschlagsstationen (Ombrometer). Deutscher Wetterdienst, Hydrometeorologie, Offenbach/M., http://www.laenderfinanzierungsprogramm.de/cms/WaBoAb_prod/WaBoAb/Vorhaben/LAWA/Vorhaben_des_ehemaligen_Ausschusses_Daten/DK_5.68/RADOLAN_Abschlussbericht_2006.pdf (last access 12 Dec 2017), 2004.
- 15 Burt, T., Boardman, J., Foster, I., Howden, N.: More rain, less soil: Long-term changes in rainfall intensity with climate change. *Earth Surf. Process. Landf.*, 41, 563-566, 2016.
- Chwala, C., Gmeiner, A., Qiu, W., Hipp, S., Nienaber, D., Siart, U., Eibert, T., Pohl, M., Seltmann, J., Fritz, J., Kunstmann, H.: Precipitation observation using micro-wave backhaul links in the alpine and pre-alpine region of southern Germany. *Hydrol. Earth Syst. Sci.*, 16, 2647-2661, <https://doi.org/10.5194/hess-16-2647-2012>, 2012.
- 20 Chwala, C., Keis, F., Kunstmann, H.: Real-time data acquisition of commercial microwave link networks for hydrometeorological applications, *Atmos. Meas. Tech.*, 9, 991-999, 2016.
- DIN – Deutsches Institut für Normung: DIN 19708: 2005-02 Bodenbeschaffenheit – Ermittlung der Erosionsgefährdung von Böden durch Wasser mit Hilfe der ABAG. Beuth-Verlag, Berlin, 2017.
- 25 Dixon, W.J., Yuen, K.: Trimming and winsorization: A review. *Statistical Papers*, 15, 157-170, 1974.
- Cerdan, O., Govers, G., Le Bissonnais, Y., Van Oost, K., Poesen, J., Saby, N., Gobin, A., Vacca, A., Quinton, J., Auerswald, K., Klik, A., Kwaad, F.J.P.M., Raclot, D., Ionita, I., Rejman, J., Rousseva, S., Muxart, T., Roxo, M.J., Dostal, T.: Rates and spatial variations of soil erosion in Europe: a study based on erosion plot data. *Geomorph.*, 122, 167–177. doi:10.1016/j.geomorph.2010.06.011, 2010.
- 30 Emde, K.: Experimentelle Untersuchungen zu Oberflächenabfluß und Bodenaustrag in Verbindung mit Starkregen bei verschiedenen Bewirtschaftungssystemen in Weinbergsarealen des oberen Rheingaus. Geisenheimer Berichte 12. Gesellschaft zur Förderung der Forschungsanstalt Geisenheim, Geisenheim, 1992.



- Fairman, J.G., Shultz, D.M., Kirshbaum, D.J., Hray, S.L., Barrett, A.I.: A radar-based rainfall climatology of Great Britain and Ireland. *Weather* 70, 153–158. DOI: 10.1002/wea.2486, 2015.
- Fiener, P., Auerswald, K.: Spatial variability of rainfall on a sub-kilometre scale. *Earth Surf. Process. Landf.*, 34, 848–859, 2009.
- 5 Fiener, P., Neuhaus, P., Botschek, J.: Long-term trends in rainfall erosivity – analysis of high resolution precipitation time series (1937–2007) from Western Germany. *Agric. Forest Meteorol.*, 171–172, 115–123, 2013.
- Fischer, F., Hauck, J., Brandhuber, R., Weigl, E., Maier, H., Auerswald, K.: Spatio-temporal variability of erosivity estimated from highly resolved and adjusted radar rain data. *Agric. Forest Meteorol.*, 223, 72–80. DOI: 10.1016/j.agrformet.2016.03.024, 2016.
- 10 Fischer, F.K., Winterrath T., Auerswald K.: Temporal and spatial scale and positional effects on rain erosivity derived from contiguous rain data. *Hydrol. Earth Syst. Sci. Discuss.*, <https://doi.org/10.5194/hess-2018-305>, 2018.
- Gallagher, N. C., Wise, G. L.: A theoretical analysis of the properties of median filters. *IEEE Transact. Acoustics, Speech, Signal Processing*, 29, 1138 - 1141, 1981.
- Gräler, B., Pebesma, E., Heuvelink, G.: Spatio-temporal interpolation using gstat. *The R Journal*, 8, 204–218, 2016.
- 15 Hardegree, S.P., Van Vactor, S.S., Levinson, D.H., Winstral, A.H.: Evaluation of NEXRAD radar precipitation products for natural resource applications. *Rangel. Ecol. Manag.*, 61, 346–353, 2008.
- Hirche, D.: Die Erosivität der Niederschläge in Niedersachsen. Diploma Thesis, University Braunschweig. 155 p., 1990.
- Koistinen, J., Michelson, D.B.: BALTEX weather radar-based precipitation products and their accuracies. *Boreal Env. Res.*, 7, 253–263, 2002.
- 20 Krajewski, W.F., Ciach, G.J., Habib, E.: An analysis of small-scale rainfall variability in different climatic regimes. *Hydrol. Sci. J.* 48, 151–162. <http://dx.doi.org/10.1623/hysj.48.2.151.44694>, 2003.
- Michelson, D., Szturc, J., Gill, R.S., Peura, M.: Community-based weather radar networking with BALTRAD. The sixth European Conference on Radar in Meteorology and Hydrology ERAD Proceedings, 6 p. http://www.erad2010.com/pdf/oral/wednesday/dataex/01_ERAD2010_0170.pdf (last access 14 May 2018), 2010.
- 25 Morgan, R.P.C., Quinton, J.N., Smith, R.E., Govers, G., Poesen, J.W.A., Auerswald, K., Chisci, G., Torri, D., Styczen, M.E.: Reply to discussion on ‘The European soil erosion model (EUROSEM): A process-based approach for predicting soil loss from fields and small catchments’. *Earth Surf. Process.*, 24, 567–568, 1999.
- Nearing, M.A., Yin, S.-Q., Borrelli, P., Polyakov, V.O.: Rainfall erosivity: An historical review. *Catena*, 157, 357–362, 2017.
- 30 Overeem, A., Leijnse, H., Uijlenhoet, R.: Country-wide rainfall maps from cellular communication networks. *Proc. Nat. Acad. Sci.*, 110, 2741–2745, 2013.
- Pedersen, L., Jensen, N.E., Christensen, L.E., Madsen, H.: Quantification of the spatial variability of rainfall based on a dense network of rain gauges. *Atmospheric Res.*, 95, 441–454. DOI: 10.1016/j.atmosres.2009.11.007, 2010.



- Peleg, N., Marra, F., Fatichi, S., Paschalis, A., Molnar, P.: Spatial variability of extreme rainfall at radar subpixel scale. *J. Hydrol.*, 556, 922–933. DOI: [10.1016/j.jhydrol.2016.05.033](https://doi.org/10.1016/j.jhydrol.2016.05.033), 2016.
- R Core Team: R: A language and environment for statistical computing. R Foundation for Statistical Computing, Vienna, Austria. URL <https://www.R-project.org/>, 2018.
- 5 Richter, G.: The soil erosion measurement station and its program. *Forschungsstelle Bodenerosion*, 10, 97–108, 1991.
- Rogler, H., Schwertmann, U.: Erosivität der Niederschläge und Isoerodentkarte Bayerns. *Zeitschrift für Kulturtechnik und Flurbereinigung*, 22, 99–112, 1981.
- Sauerborn, P.: Die Erosivität der Niederschläge in Deutschland. Ein Beitrag zur quantitativen Prognose der Bodenerosion durch Wasser in Mitteleuropa. *Bonner Bodenkundliche Abhandlungen*, 13, 1994.
- 10 Schmidt, J.: The impact of rainfall on sediment transport by sheetflow. In: Bork, H.-R., De Ploey, J., Schick, A.P. (eds): *Erosion, Transport and Deposition Processes – Theory and Models*. *Catena Suppl.*, 19, 9-17, 1991.
- Schönwiese, C.-D., Grieser, J., Trömel, S.: Secular change of extreme monthly precipitation in Europe. *Theoretical Applied Climatol.*, 75, 245-250, 2003.
- Schwertmann, U., Vogl, W., Kainz, M.: *Bodenerosion durch Wasser. Vorhersage des Abtrags und Bewertung von*
- 15 *Gegenmaßnahmen*. 2. Edition. Ulmer Verlag Stuttgart, 1990.
- Stedinger, J.R., Vogel, R.M., Foufoula-Georgiou, E.: Frequency analysis of extreme events, Chapter 18, *Handbook of Hydrology*, McGraw-Hill Book Company, D. R. Maidment, Editor-in-Chief. <https://engineering.tufts.edu/cee/people/vogel/documents/frequencyAnalysis.pdf>, 1993.
- Tukey, J.W.: *Exploratory Data Analysis*. Reading, Mass.: Addison - Wesley, 1977.
- 20 Williams, J.R., Berndt, H.D.: Sediment yield prediction based on watershed hydrology. *Trans. Amer. Soc. Agr. Eng.*, 20, 1100-1104, 1977.
- Winterrath, T., Rosenow, W., Weigl, E.: On the DWD quantitative precipitation analysis and nowcasting system for real-time application in German flood risk management. *Weather Radar and Hydrology*, IAHS Publ. 351, 323-329, 2012.
- Winterrath, T., Brendel, C., Hafer, M., Junghänel, T., Klameth, A., Walawender, E., Weigl, E., Becker, A.: Erstellung einer
- 25 radargestützten Niederschlagsklimatologie, *Berichte des Deutschen Wetterdienstes*, 251, 73 p. , 2017.
- Winterrath, T., Brendel, C., Hafer, M., Junghänel, T., Klameth, A., Lengfeld, K., Walawender, E., Weigl, E., Becker, A.: RADKLIM Version 2017.002: Reprocessed gauge-adjusted radar data, one-hour precipitation sums (RW) DOI: [10.5676/DWD/RADKLIM_RW_V2017.002](https://doi.org/10.5676/DWD/RADKLIM_RW_V2017.002), 2018.
- Wischmeier, W.H.: A rainfall erosion index for a universal soil-loss equation. *Soil Sci. Soc. Am. Proc.*, 23, 246–249, 1959.
- 30 Wischmeier, W.H., Smith, D.D.: Rainfall energy and its relationship to soil loss. *Transact. Am. Geophysical Union*, 39, 285-291, 1958.
- Wischmeier, W.H., Smith, D.D.: *Predicting rainfall erosion losses*. Agricultural Handbook, Issue 537. US Department of Agriculture: Washington, DC, 1978.

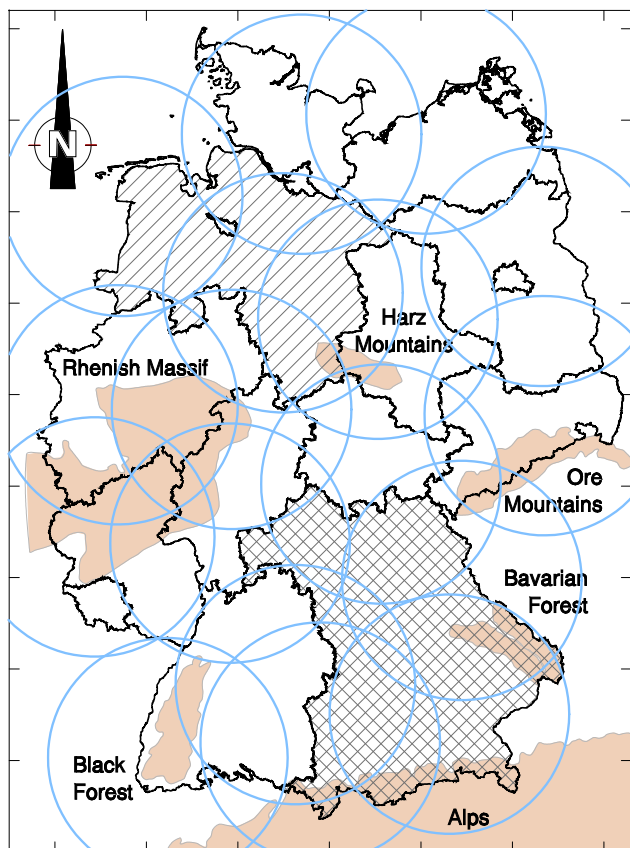


Figure 1: Coverage (blue circles) of the 17 German rain radars for a range of 128 km and the 2017 configuration (locations of some radar towers have changed over time). Black lines denote federal states; the federal states of Bavaria (cross-hatched), Lower Saxony (hatched) and selected mountain ranges (light brown) are mentioned in the text. Axis ticks represent distances of 100 km.

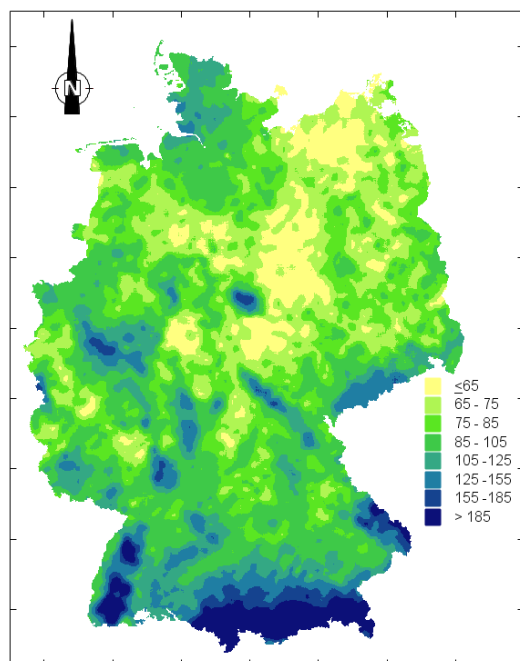


Figure 2: Erosivity map of Germany from 17 yr of radar rain data. Axes ticks represent distances of 100 km. Color classes from yellow to dark blue comprise approximately 10%, 20%, 20%, 25%, 15%, 4%, 3%, and 3% of the area, respectively. For comparison with the map before winsorizing and before kriging see Figs. A1 and A2 in the Appendix. For average values for the 294 local authority areas (average size 1214 km²), see Table A1 in the Appendix. Average values for the 11 254 communities (average size 32 km²) can be obtained at <https://www.lfl.bayern.de/iab/index.php>.

5

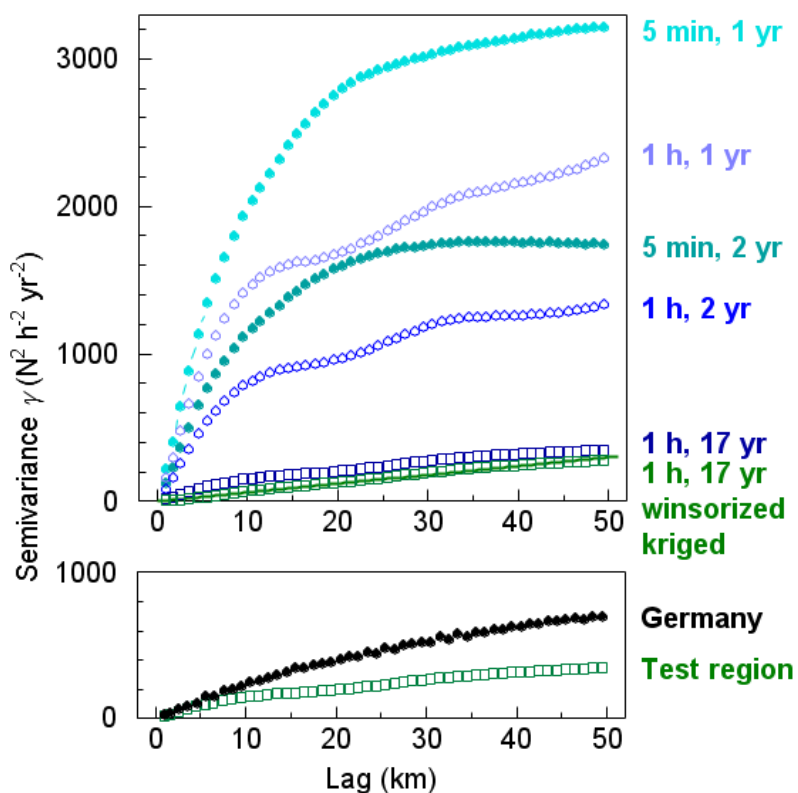
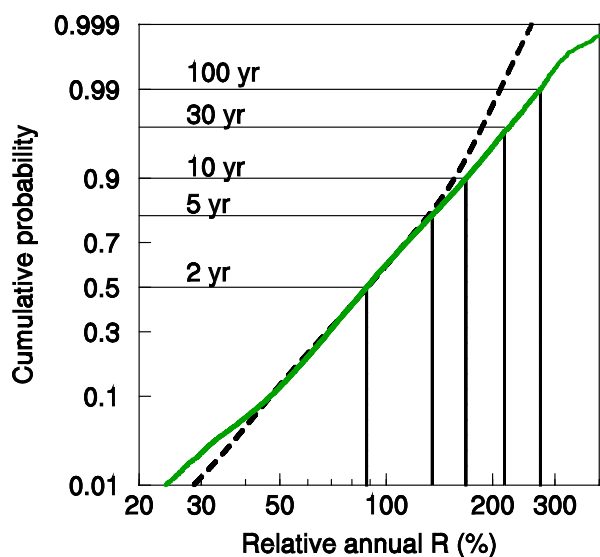
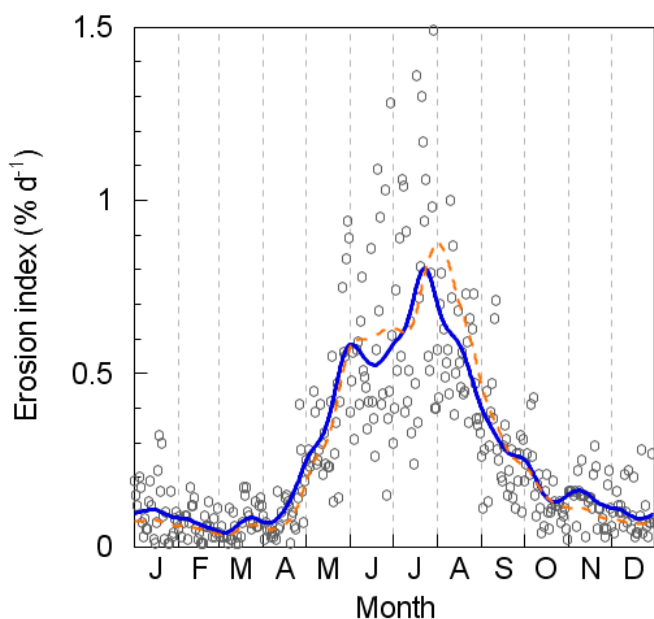


Figure 3: Upper panel: Semivariograms of erosivity for different temporal resolutions of rain data (5 min and 1 h), different averaging (1 yr, 2 yr, 17 yr), winsorizing and kriging for the test region (for selected lag classes see Table 1). The line through the semivariances of the 1 h, 17 yr, winsorized and kriged data is a linear regression through the origin ($r^2 = 0.9889$).

5 Lower panel: Comparison of semivariances for the 1 h, 17 yr and winsorized data before kriging for the test region and for the whole of Germany.



5 Figure 4: Cumulative distribution curve of the annual R factor relative to the long-term annual mean of a pixel. Dashed black line applies for erosivities derived from 1-h data for the whole of Germany and 17 yr ($n = 7.7$ million). Solid green line applies for erosivities derived from 5-min data for the test region and 2 yr ($n = 24\,770$). Straight vertical and horizontal lines indicate return periods between 2 yr and 100 yr. The y axis is probability scaled, the x axis is log scaled.



10 Figure 5: Measured (circles) and smoothed (solid blue line) daily erosion index. The daily erosion index calculated from measurements between 2001 and 2016 at 115 rain gauges distributed throughout Germany is given for comparison (orange dashed line). For C-factor calculations the smoothed values can be taken from Table A2 in the Appendix.

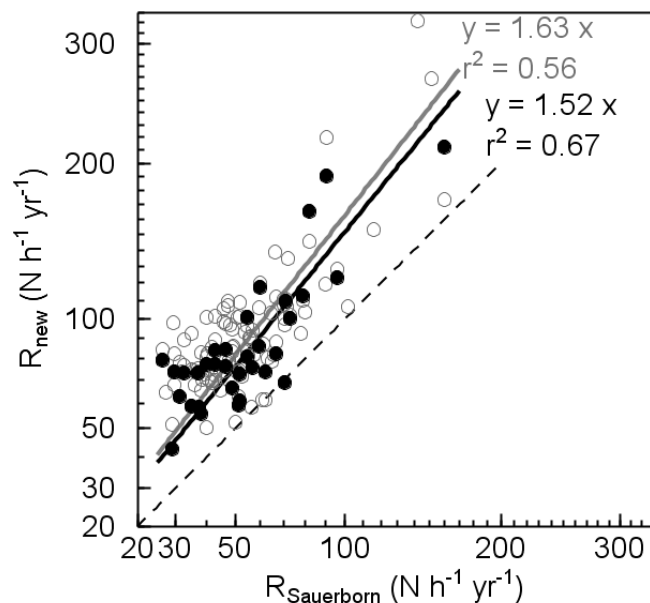


Figure 6: Comparison of erosivities reported by Sauerborn (1994), measured mainly in the 1960s to 1980s, with recent erosivities. Recent erosivities were either determined from rain gauge measurements at the same meteorological stations (mean of 2001 to 2016; taken from Fischer et al., 2018; $n = 33$; black dots) or from radar data (mean of 2001 to 2017 and all radar pixels at a distance of 1.5 km from the meteorological stations; $n = 101$, white dots). Both axes are square-root scaled to improve resolution at low erosivities. Dashed line denotes 1:1. Solid lines are regressions through the origin.

5

Table 1: Influence of temporal resolution of rain data (5 min and 1 h), averaging (1 yr, 2 yr, and 17 yr), winsorizing and kriging on the semivariance (γ) at three lags h . For complete semivariograms see Fig. 3, upper panel.

Variable	γ at $h = 10$ km ($N^2 h^{-2} yr^{-2}$)	γ at $h = 20$ km ($N^2 h^{-2} yr^{-2}$)	γ at $h = 40$ km ($N^2 h^{-2} yr^{-2}$)	Regional trend ① ($N h^{-1} yr^{-1} km^{-1}$)	Effect of violent rain cells② ($N h^{-1} yr^{-1} km^{-1}$)
5-min annual erosivity	1925	2749	3136	0.2	2.4
5-min biannual erosivity	1111	1569	1755	0.1	1.9
1-h annual erosivity	1413	1667	2147	0.3	1.8
1-h biannual erosivity	782	953	1259	0.2	1.3
1-h 17-yr mean erosivity	144	197	315	0.2	0.5
1-h winsorized mean erosivity	139	190	309	0.2	0.5
1-h kriged erosivity	60	121	239	0.2	0.3

10 ① The regional trend was calculated as the difference between the square roots of γ at lags of 40 and 20 km divided by the difference in lag of 20 km.

② The effect of violent rain cells was calculated as the square root of γ at a lag of 20 km divided by the difference in lag of 20 km minus the regional trend.



Appendix

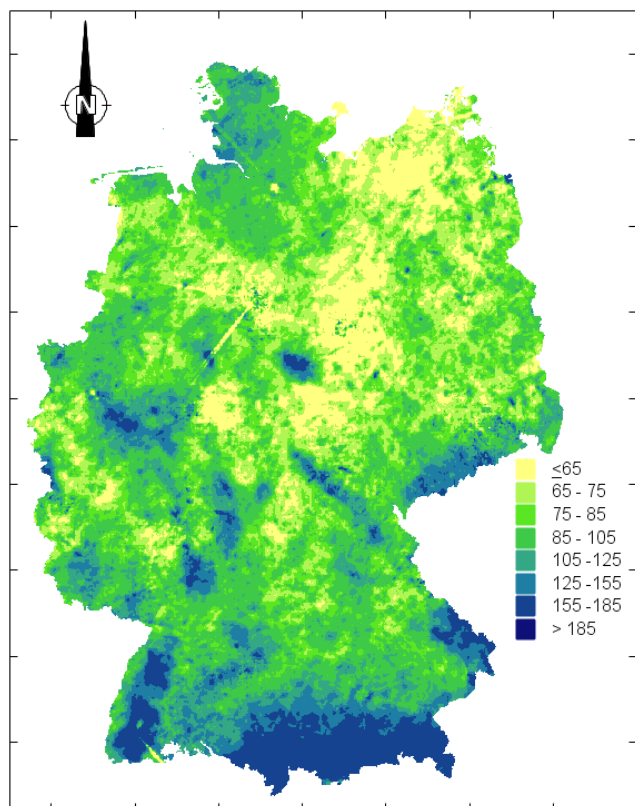


Figure A1: Erosivity map of Germany from 17 yr of radar rain data before statistical smoothing by winsorizing, removal of spikes and kriging. Axes ticks represent distances of 100 km.

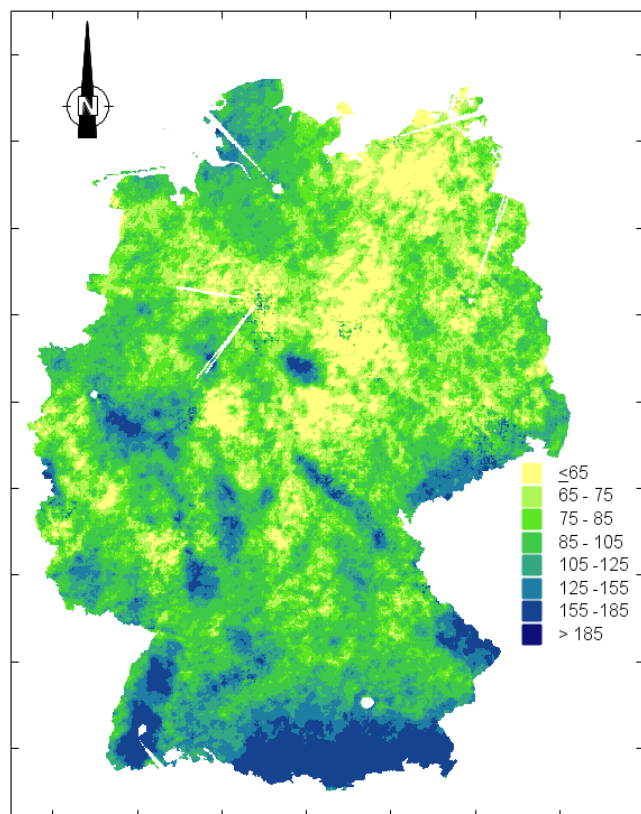


Figure A2: Erosivity map of Germany from 17 yr of radar rain data after winsorizing and removal of spokes but before kriging. Axes ticks represent distances of 100 km.

**Table A1. Mean erosivity ($\text{N h}^{-1} \text{yr}^{-1}$) of all German counties**

County (Landkreis)	Identifier	Size (km ²)	Mean R
Ahrweiler	07131001	789	74.3
Aichach-Friedberg	09771111	780	109.9
Alb-Donau-Kreis	08425002	1358	103.4
Altenburger Land	16077001	570	90.5
Altenkirchen (Westerwald)	07132001	643	100.4
Altmarkkreis Salzwedel	15081026	2304	62.2
Altötting	09171111	569	128.9
Alzey-Worms	07331001	589	68.7
Amberg	09361000	50	81.0
Amberg-Weizbach	09371111	1255	92.2
Ammerland	03451001	731	80.6
Anhalt-Bitterfeld	15082005	1461	68.0
Ansbach	09561000	2073	80.8
Aschaffenburg	09661000	762	118.7
Augsburg	09761000	1218	123.3
Aurich	03452001	1298	85.0
Bad Dürkheim	07332001	595	88.4
Bad Kissingen	09672111	1138	84.9
Bad Kreuznach	07133001	866	80.5
Bad Tölz-Wolfratshausen	09173111	1112	257.1
Baden-Baden. Stadtkreis	08211000	140	131.2
Bamberg	09461000	1222	85.5
Barnim	12060005	1481	72.7
Bautzen	14625010	2397	86.9
Bayreuth	09462000	1341	108.0
Berchtesgadener Land	09172111	840	250.0
Bergstraße	06431001	720	120.7
Berlin. Stadt	11000000	892	73.2
Bernkastel-Wittlich	07231001	1173	89.5
Biberach	08426001	1411	129.8
Bielefeld. Stadt	05711000	259	94.4
Birkenfeld	07134001	779	98.1
Böblingen	08115001	618	96.2
Bochum. Stadt	05911000	145	103.7
Bodenseekreis	08435005	666	149.3
Bonn. Stadt	05314000	142	94.5
Börde	15083020	2377	58.4
Borken	05554004	1426	94.4
Bottrop. Stadt	05512000	101	109.6
Brandenburg an der Havel. Stadt	12051000	229	78.8
Braunschweig. Stadt	03101000	192	69.3
Breisgau-Hochschwarzwald	08315003	1380	163.9

**Table A1. Mean erosivity ($N h^{-1} yr^{-1}$) of all German counties (continued)**

County (Landkreis)	Identifier	Size (km ²)	Mean R
Bremen. Stadt	04011000	326	78.0
Bremerhaven. Stadt	04012000	94	86.4
Burgenlandkreis	15084012	1419	77.0
Calw	08235006	798	105.6
Celle	03351001	1551	70.8
Cham	09372112	1527	106.1
Chemnitz. Stadt	14511000	221	107.5
Cloppenburg	03453001	1424	80.5
Coburg	09463000	639	82.4
Cochem-Zell	07135001	695	80.0
Coesfeld	05558004	1115	93.1
Cottbus. Stadt	12052000	165	74.0
Cuxhaven	03352002	2062	99.6
Dachau	09174111	580	115.1
Dahme-Spreewald	12061005	2277	79.2
Darmstadt. Wissenschaftsstadt	06411000	123	102.3
Darmstadt-Dieburg	06432001	659	91.5
Deggendorf	09271111	861	118.8
Delmenhorst. Stadt	03401000	63	69.6
Dessau-Roßlau. Stadt	15001000	246	65.0
Diepholz	03251001	1993	69.9
Dillingen a.d.Donau	09773111	792	94.7
Dingolfing-Landau	09279112	877	90.8
Dithmarschen	01051001	1444	122.5
Donau-Ries	09779111	1275	87.9
Donnersbergkreis	07333001	646	89.5
Dortmund. Stadt	05913000	280	88.7
Dresden. Stadt	14612000	328	96.9
Duisburg. Stadt	05112000	234	87.2
Düren	05358004	944	80.0
Düsseldorf. Stadt	05111000	218	75.6
Ebersberg	09175111	550	154.0
Eichsfeld	16061001	943	68.4
Eichstätt	09176111	1214	91.0
Eifelkreis Bitburg-Prüm	07232001	1634	82.0
Eisenach. Stadt	16056000	105	72.1
Elbe-Elster	12062024	1901	74.7
Emden. Stadt	03402000	112	73.3
Emmendingen	08316002	682	152.6
Emsland	03454001	2891	81.0
Ennepe-Ruhr-Kreis	05954004	412	116.1
Enzkreis	08236004	574	94.5
Erding	09177112	871	113.8

**Table A1. Mean erosivity ($\text{N h}^{-1} \text{yr}^{-1}$) of all German counties (continued)**

County (Landkreis)	Identifier	Size (km ²)	Mean R
Erfurt. Stadt	16051000	270	74.5
Erlangen	09562000	78	81.9
Erlangen-Höchstadt	09572111	565	80.2
Erzgebirgskreis	14521010	1827	136.9
Essen. Stadt	05113000	211	113.5
Esslingen	08116004	640	109.5
Euskirchen	05366004	1255	82.3
Flensburg. Stadt	01001000	57	108.8
Forchheim	09474119	643	98.3
Frankenthal (Pfalz). kreisfreie Stadt	07311000	44	80.3
Frankfurt (Oder). Stadt	12053000	148	89.6
Frankfurt am Main. Stadt	06412000	249	94.2
Freiburg im Breisgau. Stadtkreis	08311000	155	139.1
Freising	09178113	798	107.1
Freudenstadt	08237002	873	160.4
Freyung-Grafenau	09272116	985	175.0
Friesland	03455007	619	85.5
Fulda	06631001	1382	85.6
Fürstenfeldbruck	09179111	435	133.2
Fürth	09563000	371	78.3
Garmisch-Partenkirchen	09180112	1012	215.8
Gelsenkirchen. Stadt	05513000	106	108.9
Gera. Stadt	16052000	152	78.2
Germersheim	07334001	464	90.3
Gießen	06531001	857	88.0
Gifhorn	03151001	1570	72.1
Göppingen	08117001	643	119.3
Görlitz	14626010	2113	96.8
Goslar	03153002	969	122.9
Gotha	16067003	936	82.2
Göttingen	03159001	1756	92.2
Grafschaft Bentheim	03456001	985	80.6
Greiz	16076003	846	84.2
Groß-Gerau	06433001	454	73.4
Günzburg	09774111	764	112.4
Gütersloh	05754004	971	79.6
Hagen. Stadt der FernUniversität	05914000	161	104.8
Halle (Saale). Stadt	15002000	136	78.3
Hamburg. Freie und Hansestadt	02000000	753	87.7
Hameln-Pyrmont	03252001	799	79.0
Hamm. Stadt	05915000	228	77.6
Harburg	03353001	1250	88.4
Harz	15085040	2108	73.0

**Table A1. Mean erosivity ($N h^{-1} yr^{-1}$) of all German counties (continued)**

County (Landkreis)	Identifier	Size (km ²)	Mean R
Haßberge	09674111	957	83.4
Havelland	12063036	1728	74.5
Heidekreis	03358001	1883	80.3
Heidelberg. Stadtkreis	08221000	109	124.1
Heidenheim	08135010	628	99.8
Heilbronn	08125001	1100	90.5
Heilbronn. Stadtkreis	08121000	101	79.9
Heinsberg	05370004	630	71.1
Helmstedt	03154001	676	61.0
Herford	05758004	451	89.9
Herne. Stadt	05916000	52	104.6
Hersfeld-Rotenburg	06632001	1099	76.6
Herzogtum Lauenburg	01053001	1263	78.6
Hildburghausen	16069001	938	90.1
Hildesheim	03254002	1208	74.4
Hochsauerlandkreis	05958004	1963	107.5
Hochtaunuskreis	06434001	482	108.3
Hof	09464000	952	95.5
Hohenlohekreis	08126011	778	97.5
Holzminden	03255001	695	84.1
Höxter	05762004	1202	80.5
Ilm-Kreis	16070001	844	97.1
Ingolstadt	09161000	134	90.5
Jena. Stadt	16053000	115	79.0
Jerichower Land	15086005	1589	69.9
Kaiserslautern	07335002	642	97.5
Kaiserslautern. kreisfreie Stadt	07312000	141	100.7
Karlsruhe	08215007	1086	90.8
Karlsruhe. Stadtkreis	08212000	174	98.7
Kassel	06633001	1296	69.7
Kassel. documenta-Stadt	06611000	105	66.7
Kaufbeuren	09762000	40	168.0
Kelheim	09273111	1065	91.9
Kempten (Allgäu)	09763000	63	222.1
Kiel. Landeshauptstadt	01002000	120	92.5
Kitzingen	09675111	684	81.1
Kleve	05154004	1238	98.9
Koblenz. kreisfreie Stadt	07111000	106	80.2
Köln. Stadt	05315000	408	91.3
Konstanz	08335001	819	121.1
Krefeld. Stadt	05114000	137	83.1
Kronach	09476145	652	107.4
Kulmbach	09477117	658	100.4

**Table A1. Mean erosivity ($N h^{-1} yr^{-1}$) of all German counties (continued)**

County (Landkreis)	Identifier	Size (km ²)	Mean R
Kusel	07336001	575	101.2
Kyffhäuserkreis	16065001	1038	61.5
Lahn-Dill-Kreis	06532001	1067	102.7
Landau in der Pfalz. kreisfreie Stadt	07313000	83	104.7
Landkreis Rostock	13072001	3429	59.5
Landsberg am Lech	09181111	804	156.0
Landshut	09261000	1414	103.9
Leer	03457002	1089	72.8
Leipzig	14729010	1652	79.9
Leipzig. Stadt	14713000	299	87.6
Leverkusen. Stadt	05316000	79	98.0
Lichtenfels	09478111	520	80.7
Limburg-Weilburg	06533001	740	95.0
Lindau (Bodensee)	09776111	323	306.6
Lippe	05766004	1247	99.9
Lörrach	08336004	809	182.7
Lübeck. Hansestadt	01003000	212	76.1
Lüchow-Dannenberg	03354001	1227	73.6
Ludwigsburg	08118001	687	88.6
Ludwigshafen am Rhein. kreisfreie Stadt	07314000	78	87.5
Ludwigslust-Parchim	13076001	4768	71.8
Lüneburg	03355001	1327	80.4
Magdeburg. Landeshauptstadt	15003000	201	54.2
Main-Kinzig-Kreis	06435001	1398	110.4
Main-Spessart	09677114	1323	95.1
Main-Tauber-Kreis	08128006	1306	93.8
Main-Taunus-Kreis	06436001	222	102.2
Mainz. kreisfreie Stadt	07315000	98	68.4
Mainz-Bingen	07339001	607	68.8
Mannheim. Stadtkreis	08222000	145	92.9
Mansfeld-Südharz	15087010	1456	66.8
Marburg-Biedenkopf	06534001	1264	83.0
Märkischer Kreis	05962004	1064	121.3
Märkisch-Oderland	12064009	2159	80.6
Mayen-Koblenz	07137001	819	69.6
Mecklenburgische Seenplatte	13071001	5496	67.2
Meißen	14627010	1458	76.5
Memmingen	09764000	70	157.0
Merzig-Wadern	10042111	559	108.4
Mettmann	05158004	409	101.9
Miesbach	09182111	867	281.4
Miltenberg	09676111	716	105.2
Minden-Lübbecke	05770004	1153	77.0

**Table A1. Mean erosivity ($N h^{-1} yr^{-1}$) of all German counties (continued)**

County (Landkreis)	Identifier	Size (km ²)	Mean R
Mittelsachsen	14522010	2115	102.9
Mönchengladbach. Stadt	05116000	171	76.8
Mühdorf a.Inn	09183112	805	110.8
Mülheim an der Ruhr. Stadt	05117000	92	101.4
München	09184112	664	161.1
München. Landeshauptstadt	09162000	311	149.4
Münster. Stadt	05515000	304	88.9
Neckar-Odenwald-Kreis	08225001	1127	104.4
Neuburg-Schrobenhausen	09185113	740	93.8
Neumarkt i.d.OPf.	09373112	1345	92.8
Neumünster. Stadt	01004000	71	100.2
Neunkirchen	10043111	249	117.5
Neustadt a.d.Aisch-Bad Windsheim	09575112	1268	81.8
Neustadt a.d.Waldnaab	09374111	1428	88.8
Neustadt an der Weinstraße. kreisfreie Stadt	07316000	118	92.1
Neu-Ulm	09775111	516	121.0
Neuwied	07138002	629	80.4
Nienburg (Weser)	03256001	1403	66.6
Nordfriesland	01054001	2090	101.3
Nordhausen	16062002	714	63.2
Nordsachsen	14730010	2028	73.1
Nordwestmecklenburg	13074001	2125	68.6
Northeim	03155001	1270	81.7
Nürnberg	09564000	188	82.7
Nürnberger Land	09574111	798	103.9
Oberallgäu	09780112	1529	315.6
Oberbergischer Kreis	05374004	920	144.4
Oberhausen. Stadt	05119000	78	103.9
Oberhavel	12065036	1808	71.3
Oberspreewald-Lausitz	12066008	1224	75.4
Odenwaldkreis	06437001	626	124.6
Oder-Spree	12067024	2259	81.0
Offenbach	06438001	357	83.0
Offenbach am Main. Stadt	06413000	45	88.5
Oldenburg	03458001	1067	73.1
Oldenburg (Oldenburg). Stadt	03403000	104	78.8
Olpe	05966004	713	124.0
Ortenaukreis	08317001	1864	137.3
Osnabrück	03459001	2125	83.1
Osnabrück. Stadt	03404000	120	85.0
Ostalbkreis	08136002	1511	106.0
Ostallgäu	09777111	1394	215.5
Osterholz	03356001	654	84.5

**Table A1. Mean erosivity ($\text{N h}^{-1} \text{yr}^{-1}$) of all German counties (continued)**

County (Landkreis)	Identifier	Size (km^2)	Mean R
Ostholstein	01055001	1394	77.3
Ostprignitz-Ruppin	12068052	2526	77.0
Paderborn	05774004	1248	91.8
Passau	09262000	1600	121.0
Peine	03157001	536	65.8
Pfaffenhofen a.d.Ilm	09186113	761	100.8
Pforzheim. Stadtkreis	08231000	98	89.3
Pinneberg	01056001	664	97.6
Pirmasens. kreisfreie Stadt	07317000	62	99.4
Plön	01057001	1084	83.3
Potsdam. Stadt	12054000	187	70.5
Potsdam-Mittelmark	12069017	2593	78.3
Prignitz	12070008	2139	69.6
Rastatt	08216002	740	126.3
Ravensburg	08436001	1633	178.3
Recklinghausen	05562004	763	100.3
Regen	09276111	975	164.4
Regensburg	09362000	1473	84.4
Region Hannover	03241001	2299	70.8
Regionalverband Saarbrücken	10041100	413	103.7
Remscheid. Stadt	05120000	74	150.4
Rems-Murr-Kreis	08119001	858	119.4
Rendsburg-Eckernförde	01058001	2190	104.7
Reutlingen	08415014	1093	119.8
Rhein-Erft-Kreis	05362004	705	76.4
Rheingau-Taunus-Kreis	06439001	814	88.0
Rhein-Hunsrück-Kreis	07140001	994	84.1
Rheinisch-Bergischer Kreis	05378004	439	120.3
Rhein-Kreis Neuss	05162004	579	72.2
Rhein-Lahn-Kreis	07141001	783	87.8
Rhein-Neckar-Kreis	08226003	1062	114.3
Rhein-Pfalz-Kreis	07338001	305	88.5
Rhein-Sieg-Kreis	05382004	1155	96.8
Rhön-Grabfeld	09673113	1022	74.7
Rosenheim	09163000	1477	210.4
Rostock	13003000	181	68.4
Rotenburg (Wümme)	03357001	2075	92.6
Roth	09576111	895	84.9
Rottal-Inn	09277111	1281	102.6
Rottweil	08325001	771	115.4
Saale-Holzland-Kreis	16074001	816	85.5
Saalekreis	15088020	1440	73.1
Saale-Orla-Kreis	16075002	1152	84.8

**Table A1. Mean erosivity ($N h^{-1} yr^{-1}$) of all German counties (continued)**

County (Landkreis)	Identifier	Size (km ²)	Mean R
Saalfeld-Rudolstadt	16073001	1036	87.1
Saarlouis	10044111	461	105.3
Saarpfalz-Kreis	10045111	420	101.3
Sächsische Schweiz-Osterzgebirge	14628010	1654	111.7
Salzgitter. Stadt	03102000	225	73.6
Salzlandkreis	15089005	1435	61.5
Schaumburg	03257001	677	81.9
Schleswig-Flensburg	01059001	2072	106.8
Schmalkalden-Meiningen	16066001	1211	84.7
Schwabach	09565000	41	73.6
Schwäbisch Hall	08127008	1485	94.6
Schwalm-Eder-Kreis	06634001	1541	70.7
Schwandorf	09376112	1458	81.5
Schwarzwald-Baar-Kreis	08326003	1028	135.6
Schweinfurt	09662000	877	71.0
Schwerin	13004000	130	64.8
Segeberg	01060002	1346	92.6
Siegen-Wittgenstein	05970004	1136	121.3
Sigmaringen	08437005	1206	118.3
Soest	05974004	1332	88.1
Solingen. Klingenstein	05122000	89	115.1
Sömmerda	16068001	807	64.6
Sonneberg	16072001	433	125.5
Speyer. kreisfreie Stadt	07318000	43	89.0
Spree-Neiße	12071028	1658	77.5
St. Wendel	10046111	478	122.4
Stade	03359001	1268	97.1
Städteregion Aachen	05334002	707	105.9
Starnberg	09188113	487	169.0
Steinburg	01061001	1057	107.7
Steinfurt	05566004	1800	95.6
Stendal	15090003	2437	64.5
Stormarn	01062001	766	87.6
Straubing	09263000	67	90.5
Straubing-Bogen	09278112	1201	103.8
Stuttgart. Stadtkreis	08111000	210	92.0
Südliche Weinstraße	07337001	641	104.2
Südwestpfalz	07340001	957	109.7
Suhl. Stadt	16054000	102	123.8
Teltow-Fläming	12072002	2104	73.0
Tirschenreuth	09377112	1085	96.5
Traunstein	09189111	1533	232.0
Trier. kreisfreie Stadt	07211000	116	77.3

**Table A1. Mean erosivity ($N h^{-1} yr^{-1}$) of all German counties (continued)**

County (Landkreis)	Identifier	Size (km ²)	Mean R
Trier-Saarburg	07235001	1109	92.8
Tübingen	08416006	521	114.2
Tuttlingen	08327002	735	124.3
Uckermark	12073008	3077	74.2
Uelzen	03360001	1463	79.2
Ulm. Stadtkreis	08421000	119	93.7
Unna	05978004	544	83.6
Unstrut-Hainich-Kreis	16064001	979	63.2
Unterallgäu	09778111	1230	161.8
Vechta	03460001	815	73.2
Verden	03361001	790	76.5
Viersen	05166004	566	78.0
Vogelsbergkreis	06535001	1460	95.3
Vogtlandkreis	14523010	1412	101.5
Vorpommern-Greifswald	13075001	3953	72.1
Vorpommern-Rügen	13073001	3213	66.2
Vulkaneifel	07233002	915	88.4
Waldeck-Frankenberg	06635001	1850	72.8
Waldshut	08337002	1133	166.8
Warendorf	05570004	1321	75.6
Wartburgkreis	16063003	1307	75.7
Weiden i.d.OPf.	09363000	71	91.7
Weilheim-Schongau	09190111	968	214.4
Weimar. Stadt	16055000	84	70.6
Weimarer Land	16071001	804	73.8
Weißenburg-Gunzenhausen	09577111	971	94.1
Werra-Meißner-Kreis	06636001	1025	73.9
Wesel	05170004	1046	92.7
Wesermarsch	03461001	830	77.9
Westerwaldkreis	07143001	992	100.5
Wetteraukreis	06440001	1102	97.0
Wiesbaden. Landeshauptstadt	06414000	204	79.4
Wilhelmshaven. Stadt	03405000	108	94.8
Wittenberg	15091010	1943	77.8
Wittmund	03462001	661	96.6
Wolfenbüttel	03158002	724	71.7
Wolfsburg. Stadt	03103000	205	66.3
Worms. kreisfreie Stadt	07319000	109	71.7
Wunsiedel i.Fichtelgebirge	09479111	606	92.9
Wuppertal. Stadt	05124000	169	128.8
Würzburg	09663000	1055	85.0
Zollernalbkreis	08417002	918	118.0



Table A1. Mean erosivity ($\text{N h}^{-1} \text{yr}^{-1}$) of all German counties (continued)

County (Landkreis)	Identifier	Size (km^2)	Mean R
Zweibrücken. kreisfreie Stadt	07320000	71	90.4
Zwickau	14524010	950	102.4

**Table A2. Daily erosion index**

Date	Daily erosi- vity (%)	Erosi- vity since 1 Jan (%)									
1 Jan	0.09	0.1	1 Apr	0.07	6.9	1 Jul	0.58	39.3	1 Oct	0.25	87.8
2 Jan	0.10	0.2	2 Apr	0.07	7.0	2 Jul	0.58	39.9	2 Oct	0.25	88.0
3 Jan	0.10	0.3	3 Apr	0.07	7.1	3 Jul	0.59	40.5	3 Oct	0.25	88.3
4 Jan	0.10	0.4	4 Apr	0.07	7.1	4 Jul	0.59	41.1	4 Oct	0.24	88.5
5 Jan	0.10	0.5	5 Apr	0.07	7.2	5 Jul	0.60	41.7	5 Oct	0.23	88.8
6 Jan	0.10	0.6	6 Apr	0.07	7.3	6 Jul	0.60	42.3	6 Oct	0.23	89.0
7 Jan	0.10	0.7	7 Apr	0.07	7.4	7 Jul	0.61	42.9	7 Oct	0.22	89.2
8 Jan	0.10	0.8	8 Apr	0.07	7.4	8 Jul	0.61	43.5	8 Oct	0.21	89.4
9 Jan	0.10	0.9	9 Apr	0.07	7.5	9 Jul	0.62	44.1	9 Oct	0.20	89.6
10 Jan	0.10	1.0	10 Apr	0.07	7.6	10 Jul	0.63	44.8	10 Oct	0.19	89.8
11 Jan	0.10	1.1	11 Apr	0.08	7.6	11 Jul	0.64	45.4	11 Oct	0.18	90.0
12 Jan	0.11	1.2	12 Apr	0.08	7.7	12 Jul	0.65	46.1	12 Oct	0.17	90.2
13 Jan	0.11	1.3	13 Apr	0.09	7.8	13 Jul	0.67	46.7	13 Oct	0.17	90.3
14 Jan	0.11	1.4	14 Apr	0.09	7.9	14 Jul	0.68	47.4	14 Oct	0.16	90.5
15 Jan	0.11	1.5	15 Apr	0.10	8.0	15 Jul	0.70	48.1	15 Oct	0.15	90.6
16 Jan	0.11	1.6	16 Apr	0.10	8.1	16 Jul	0.71	48.8	16 Oct	0.15	90.8
17 Jan	0.11	1.7	17 Apr	0.11	8.2	17 Jul	0.73	49.5	17 Oct	0.14	90.9
18 Jan	0.10	1.8	18 Apr	0.11	8.3	18 Jul	0.75	50.3	18 Oct	0.14	91.1
19 Jan	0.10	1.9	19 Apr	0.12	8.4	19 Jul	0.76	51.1	19 Oct	0.13	91.2
20 Jan	0.10	2.0	20 Apr	0.13	8.6	20 Jul	0.78	51.8	20 Oct	0.13	91.3
21 Jan	0.10	2.1	21 Apr	0.14	8.7	21 Jul	0.79	52.6	21 Oct	0.13	91.5
22 Jan	0.10	2.2	22 Apr	0.15	8.9	22 Jul	0.80	53.4	22 Oct	0.13	91.6
23 Jan	0.10	2.3	23 Apr	0.15	9.0	23 Jul	0.80	54.2	23 Oct	0.13	91.7
24 Jan	0.09	2.4	24 Apr	0.16	9.2	24 Jul	0.80	55.0	24 Oct	0.13	91.9
25 Jan	0.09	2.5	25 Apr	0.17	9.3	25 Jul	0.80	55.8	25 Oct	0.13	92.0
26 Jan	0.09	2.6	26 Apr	0.18	9.5	26 Jul	0.79	56.6	26 Oct	0.13	92.1
27 Jan	0.09	2.7	27 Apr	0.20	9.7	27 Jul	0.79	57.4	27 Oct	0.13	92.2
28 Jan	0.09	2.8	28 Apr	0.21	9.9	28 Jul	0.77	58.2	28 Oct	0.14	92.4
29 Jan	0.09	2.9	29 Apr	0.22	10.2	29 Jul	0.76	58.9	29 Oct	0.14	92.5
30 Jan	0.08	3.0	30 Apr	0.23	10.4	30 Jul	0.74	59.7	30 Oct	0.14	92.7
31 Jan	0.08	3.0				31 Jul	0.73	60.4	31 Oct	0.14	92.8

**Table A2. Daily erosion index (continued)**

Date	Daily erosi- vity (%)	Erosi- vity since 1 Jan (%)									
1 Feb	0.08	3.1	1 May	0.24	10.6	1 Aug	0.71	61.1	1 Nov	0.15	93.0
2 Feb	0.08	3.2	2 May	0.25	10.9	2 Aug	0.70	61.8	2 Nov	0.15	93.1
3 Feb	0.08	3.3	3 May	0.26	11.1	3 Aug	0.68	62.5	3 Nov	0.15	93.3
4 Feb	0.08	3.4	4 May	0.26	11.4	4 Aug	0.67	63.2	4 Nov	0.16	93.4
5 Feb	0.08	3.5	5 May	0.27	11.7	5 Aug	0.66	63.8	5 Nov	0.16	93.6
6 Feb	0.08	3.5	6 May	0.28	11.9	6 Aug	0.65	64.5	6 Nov	0.16	93.7
7 Feb	0.08	3.6	7 May	0.28	12.2	7 Aug	0.64	65.1	7 Nov	0.16	93.9
8 Feb	0.08	3.7	8 May	0.29	12.5	8 Aug	0.63	65.8	8 Nov	0.16	94.1
9 Feb	0.08	3.8	9 May	0.29	12.8	9 Aug	0.63	66.4	9 Nov	0.16	94.2
10 Feb	0.08	3.8	10 May	0.30	13.1	10 Aug	0.62	67.0	10 Nov	0.16	94.4
11 Feb	0.07	3.9	11 May	0.30	13.4	11 Aug	0.62	67.6	11 Nov	0.16	94.5
12 Feb	0.07	4.0	12 May	0.31	13.7	12 Aug	0.61	68.2	12 Nov	0.16	94.7
13 Feb	0.07	4.1	13 May	0.32	14.0	13 Aug	0.61	68.9	13 Nov	0.16	94.9
14 Feb	0.07	4.1	14 May	0.33	14.4	14 Aug	0.60	69.5	14 Nov	0.15	95.0
15 Feb	0.07	4.2	15 May	0.34	14.7	15 Aug	0.60	70.1	15 Nov	0.15	95.2
16 Feb	0.07	4.3	16 May	0.35	15.0	16 Aug	0.59	70.6	16 Nov	0.15	95.3
17 Feb	0.06	4.3	17 May	0.36	15.4	17 Aug	0.59	71.2	17 Nov	0.15	95.5
18 Feb	0.06	4.4	18 May	0.37	15.8	18 Aug	0.58	71.8	18 Nov	0.14	95.6
19 Feb	0.06	4.5	19 May	0.39	16.2	19 Aug	0.57	72.4	19 Nov	0.14	95.7
20 Feb	0.06	4.5	20 May	0.41	16.6	20 Aug	0.56	72.9	20 Nov	0.13	95.9
21 Feb	0.06	4.6	21 May	0.43	17.0	21 Aug	0.55	73.5	21 Nov	0.13	96.0
22 Feb	0.06	4.6	22 May	0.45	17.4	22 Aug	0.54	74.0	22 Nov	0.13	96.1
23 Feb	0.05	4.7	23 May	0.47	17.9	23 Aug	0.52	74.5	23 Nov	0.13	96.3
24 Feb	0.05	4.7	24 May	0.48	18.4	24 Aug	0.51	75.1	24 Nov	0.12	96.4
25 Feb	0.05	4.8	25 May	0.50	18.9	25 Aug	0.50	75.6	25 Nov	0.12	96.5
26 Feb	0.05	4.8	26 May	0.52	19.4	26 Aug	0.48	76.0	26 Nov	0.12	96.6
27 Feb	0.05	4.9	27 May	0.53	19.9	27 Aug	0.47	76.5	27 Nov	0.12	96.7
28 Feb	0.05	4.9	28 May	0.55	20.5	28 Aug	0.46	77.0	28 Nov	0.12	96.9
			29 May	0.56	21.1	29 Aug	0.44	77.4	29 Nov	0.11	97.0
			30 May	0.57	21.6	30 Aug	0.43	77.8	30 Nov	0.11	97.1
			31 May	0.58	22.2	31 Aug	0.42	78.3			

**Table A2. Daily erosion index (continued)**

Date	Daily erosi- vity (%)	Erosi- vity since 1 Jan (%)									
1 Mar	0.04	5.0	1 Jun	0.58	22.8	1 Sep	0.41	78.7	1 Dec	0.11	97.2
2 Mar	0.04	5.0	2 Jun	0.58	23.4	2 Sep	0.40	79.1	2 Dec	0.11	97.3
3 Mar	0.04	5.1	3 Jun	0.58	24.0	3 Sep	0.39	79.4	3 Dec	0.11	97.4
4 Mar	0.04	5.1	4 Jun	0.58	24.5	4 Sep	0.38	79.8	4 Dec	0.11	97.5
5 Mar	0.04	5.1	5 Jun	0.58	25.1	5 Sep	0.37	80.2	5 Dec	0.11	97.6
6 Mar	0.04	5.2	6 Jun	0.58	25.7	6 Sep	0.36	80.6	6 Dec	0.11	97.7
7 Mar	0.04	5.2	7 Jun	0.57	26.3	7 Sep	0.35	80.9	7 Dec	0.11	97.9
8 Mar	0.04	5.3	8 Jun	0.57	26.8	8 Sep	0.35	81.3	8 Dec	0.11	98.0
9 Mar	0.04	5.3	9 Jun	0.56	27.4	9 Sep	0.34	81.6	9 Dec	0.10	98.1
10 Mar	0.05	5.4	10 Jun	0.55	27.9	10 Sep	0.33	81.9	10 Dec	0.10	98.2
11 Mar	0.05	5.4	11 Jun	0.55	28.5	11 Sep	0.33	82.3	11 Dec	0.10	98.3
12 Mar	0.05	5.5	12 Jun	0.54	29.0	12 Sep	0.32	82.6	12 Dec	0.10	98.4
13 Mar	0.05	5.5	13 Jun	0.54	29.6	13 Sep	0.31	82.9	13 Dec	0.09	98.5
14 Mar	0.06	5.6	14 Jun	0.53	30.1	14 Sep	0.31	83.2	14 Dec	0.09	98.6
15 Mar	0.06	5.6	15 Jun	0.53	30.6	15 Sep	0.30	83.5	15 Dec	0.09	98.6
16 Mar	0.06	5.7	16 Jun	0.53	31.2	16 Sep	0.29	83.8	16 Dec	0.09	98.7
17 Mar	0.07	5.8	17 Jun	0.53	31.7	17 Sep	0.29	84.1	17 Dec	0.09	98.8
18 Mar	0.07	5.8	18 Jun	0.52	32.2	18 Sep	0.28	84.4	18 Dec	0.08	98.9
19 Mar	0.07	5.9	19 Jun	0.52	32.7	19 Sep	0.28	84.6	19 Dec	0.08	99.0
20 Mar	0.08	6.0	20 Jun	0.52	33.3	20 Sep	0.27	84.9	20 Dec	0.08	99.1
21 Mar	0.08	6.1	21 Jun	0.53	33.8	21 Sep	0.27	85.2	21 Dec	0.08	99.1
22 Mar	0.08	6.1	22 Jun	0.53	34.3	22 Sep	0.27	85.4	22 Dec	0.08	99.2
23 Mar	0.08	6.2	23 Jun	0.53	34.9	23 Sep	0.26	85.7	23 Dec	0.08	99.3
24 Mar	0.08	6.3	24 Jun	0.54	35.4	24 Sep	0.26	86.0	24 Dec	0.08	99.4
25 Mar	0.08	6.4	25 Jun	0.54	35.9	25 Sep	0.26	86.2	25 Dec	0.08	99.5
26 Mar	0.08	6.5	26 Jun	0.55	36.5	26 Sep	0.26	86.5	26 Dec	0.08	99.6
27 Mar	0.08	6.6	27 Jun	0.55	37.0	27 Sep	0.26	86.8	27 Dec	0.09	99.6
28 Mar	0.08	6.6	28 Jun	0.56	37.6	28 Sep	0.26	87.0	28 Dec	0.09	99.7
29 Mar	0.08	6.7	29 Jun	0.57	38.2	29 Sep	0.26	87.3	29 Dec	0.09	99.8
30 Mar	0.08	6.8	30 Jun	0.57	38.7	30 Sep	0.26	87.5	30 Dec	0.09	99.9
31 Mar	0.07	6.9							31 Dec	0.09	100.0